IOPscience iopscience.iop.org

Home Search Collections Journals About Contact us My IOPscience

Electron - nuclear double-resonance study of a substitutional Fe^{3+} defect complex in x-irradiated NaCl crystals

This article has been downloaded from IOPscience. Please scroll down to see the full text article.

1997 J. Phys.: Condens. Matter 9 7631

(http://iopscience.iop.org/0953-8984/9/36/012)

View the table of contents for this issue, or go to the journal homepage for more

Download details:
IP Address: 171.66.16.209
The article was downloaded on 14/05/2010 at 10:28

Please note that terms and conditions apply.

J. Phys.: Condens. Matter **9** (1997) 7631–7642. Printed in the UK PII: S0953-8984(97)84178-1

Electron–nuclear double-resonance study of a substitutional Fe^{3+} defect complex in x-irradiated NaCl crystals

Th Pawlik, S V Nistor† and J-M Spaeth

University of Paderborn, Fachbereich 6—Physik, Warburger Strasse 100, D-33898 Paderborn, Germany

Received 14 May 1997

Abstract. We present an EPR/ENDOR study of the so-called Fe^{3+}(I) centres produced by x-irradiation at $T \leqslant 200$ K of NaCl:Fe crystals grown in a chlorine atmosphere which had previously been studied by means of EPR. It is shown that the Fe^{3+}(I) centres each consist of a substitutional Fe^{3+} ion with a defect in the nearest-neighbour chlorine site. The defect, which is responsible for the very large axial zero-field splitting of the Fe^{3+}(I) centres, is either an interstitial Cl_i^- ion, which forms a weakly bound $(Cl_i^-)_2$ split interstitial with the nearby substitutional Cl^- ion, or a divacancy consisting of a nearest-neighbour Cl^- vacancy and a Na^+ vacancy next to it on the same axis. At room temperature the Fe^{3+}(I) centres are transformed into cubic Fe^{3+} centres, in which the Fe^{3+} ion is situated in an interstitial site.

1. Introduction

Electron paramagnetic resonance (EPR) studies on x- or γ-irradiated NaCl:Fe single crystals have shown that iron, which is incorporated into the crystal lattice as Fe^{2+}, can act either as an electron trap [1, 2] or as a trap for both electrons and holes [3, 4], resulting in several Fe^+ and Fe^{3+} paramagnetic species. The electron/hole trapping properties of the Fe^{2+} ions depend on the preparation conditions. Electron-trapping Fe^{2+} centres are produced in NaCl:Fe crystals conventionally grown (in air, in an inert atmosphere or in vacuum), as well as in chlorinated crystals (grown in a chlorine atmosphere). Hole-trapping Fe^{2+} centres are produced only in chlorinated NaCl:Fe crystals.

Pulse-annealing experiments on samples irradiated at liquid nitrogen temperature (LNT) have shown that the trapped-electron Fe^+ centres result from electron trapping at substitutional Fe^{2+} ions with a charge-compensating cation vacancy situated either in the nearest neighbourhood (nn), or in the next-nearest neighbourhood (nnn), or further away [1, 2].

The Fe^{3+} trapped-hole centres with orthorhombic symmetry (local axes $\langle 110\rangle$, $\langle 1\bar{1}0\rangle$, $\langle 001\rangle$), which are produced [3, 4] by irradiation at LNT and subsequent annealing up to $T = 250$ K, exhibit a very large axial zero-field-splitting (ZFS) parameter B_2^0, up to one order of magnitude larger than those for the isoelectronic Mn^{2+} centres in NaCl [5]. The only exception is the so-called Fe^{3+}(IV) centre observed in small amounts after irradiation at LNT and subsequent annealing at 135 K $< T <$ 185 K [4], which exhibits a local $\langle 001\rangle$ axial symmetry and a small B_2^0-parameter (table 1).

† Permanent address: Institute of Atomic Physics (IFTM), PO Box MG-6, Magurele, Bucuresti-76900, Romania.

0953-8984/97/367631+12$19.50 © 1997 IOP Publishing Ltd

Table 1. Spin-Hamiltonian parameters of the Fe^{3+}(I) and Fe^{3+}(IV) centres in NaCl (at $T = 140$ K) and of the isoelectronic, non-cubic Mn^{2+} centres (at $T = 77$ K), in NaCl. The ZFS parameters B_n^m are given in mT.

Centre	g	B_2^0	B_2^2	B_4^0	B_4^2	B_4^4
Fe^{3+}(I)[a]	2.0107	52.1	13.2	−0.0025	0.013	0.052
Fe^{3+}(IV)[b]	2.0115	5.22	—	—	—	0.079
$Mn^{2+}v_c$(nn)[c]	2.0021	4.81	4.35	—	—	0.006
$Mn^{2+}v_c$(nnn)[d]	2.0022	4.67	—	—	—	—
$Mn^{2+}I_z$[e]	1.95	49.61	10.6	—	—	0.171

[a]The estimated errors are: ±0.0003 (g), ±0.1 (B_2^0), ±3 (B_2^2), ±0.02 (B_4^0), ±0.01 (B_4^2), ±0.04 (B_4^4).
[b]Reference [4]. Axial ⟨001⟩ symmetry. $Fe^{3+}v_c$(nnn) structure.
[c]Reference [5]. Orthorhombic ⟨110⟩, ⟨1$\bar{1}$0⟩, ⟨001⟩ symmetry.
[d]Reference [5]. Axial ⟨001⟩ symmetry.
[e]Reference [11]. Orthorhombic ⟨100⟩, ⟨010⟩, ⟨001⟩ symmetry.

By further annealing above 250 K or by x-irradiation at room temperature (RT), the orthorhombic Fe^{3+} centres are converted into cubic Fe^{3+}_{cub} centres. As suggested previously from the analysis of the EPR superhyperfine (shf) structure [6], and recently confirmed by electron–nuclear double-resonance (ENDOR) spectroscopy [7], the Fe^{3+}_{cub} centre consists of an interstitial Fe^{3+} ion with its four nearest Na^+ neighbours missing. As far as we are aware, the presence of such an interstitial cation in the compact NaCl lattice which is known to exhibit a predominant Schottky type of disorder [8] had not been reported before. This result raises the question of whether iron goes into the interstitial position during irradiation or whether it is already present as Fe^{2+}_i in the as-grown chlorinated NaCl:Fe crystals. Moreover, the origin of the very strong axial crystal-field component exhibited by the low-temperature Fe^{3+} centres has not yet been explained.

In an effort to understand these aspects, we performed a combined EPR/ENDOR study of the so-called Fe^{3+}(I) centre [4] observed in chlorinated NaCl:Fe crystals. The structure of the Fe^{3+}(I) centre is expected to be the same as that of its Fe^{2+}(I) precursor, from which it is produced by hole trapping [4].

2. Experimental procedure

The samples were cleaved from the same NaCl:Fe single crystal as was used in all of the previous EPR studies described in [1–4, 6, 7]. The sample was boule doped in the melt with $FeCl_2$ and grown by the Bridgman technique in a chlorine atmosphere. Such treatment is known to eliminate any trace of oxygen or oxygen-containing anion impurities. Strong signals attributed to the Fe^{3+}(I) centres were obtained by x-irradiation (W anode, 60 kV) of the crystals at LNT for about 15 minutes, followed by a brief (≈10 min) annealing at 190 K $\leqslant T \leqslant$ 200 K. At this temperature, the now mobile self-trapped holes (V_K centres) are trapped by the precursor Fe^{2+}(I) centre, resulting in a maximum concentration of Fe^{3+}(I) centres. Just before irradiation, the samples were annealed at $T = 773$ K for 10 minutes in an alumina boat and quenched to RT on a metal block in order to disperse the Fe^{2+} ions which have a tendency to agglomerate in the NaCl lattice [9].

The EPR measurements were performed in X-band (9 GHz) and Q-band (35 GHz) Varian E-12 spectrometers equipped with the corresponding microwave bridges and nitrogen-gas-flow cooling systems.

Stationary ENDOR experiments, as well as some EPR measurements, were performed with the same custom-built, computer-controlled X-band spectrometer as was employed in our previous studies on Fe^{3+}_{cub} centres [7]. The best stationary ENDOR spectra were obtained at $T = 15$ K.

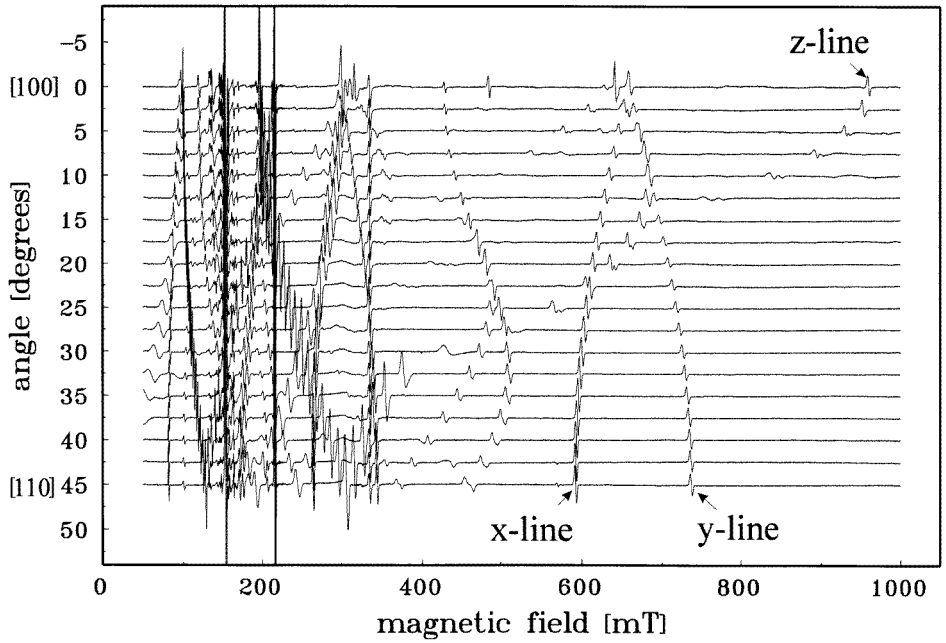

Figure 1. X-band ($\nu = 9.39$ GHz) EPR angular variation (at $T = 20$ K) of the Fe^{3+}(I) centres in a chlorinated NaCl:Fe crystal after x-irradiation at LNT and pulse annealing at $T = 200$ K for five minutes.

3. Results

3.1. EPR measurements

The X-band EPR spectrum of the Fe^{3+}(I) centres extends over a large magnetic field range (50 to 950 mT) and exhibits a large number of lines (figure 1). Their strong anisotropy, in both intensity and position, results in a very difficult identification of the corresponding EPR transitions.

These difficulties were removed by performing EPR measurements in the Q band [4]. The resulting spectra exhibit the well-known five-line multiplet structure from a ^{6}S paramagnetic ion in an axial crystal field along a $\langle 001 \rangle$ direction, perturbed by an orthorhombic component along a set of perpendicular $\langle 110 \rangle$ and $\langle 1\bar{1}0 \rangle$ axes [10].

The observed EPR spectra of the Fe^{3+}(I) centre are described quantitatively by the following spin Hamiltonian:

$$\mathcal{H} = g\mu_B \boldsymbol{H} \cdot \boldsymbol{S} + B_2^0 \hat{O}_2^0 + B_2^2 \hat{O}_2^2 + B_4^0 \hat{O}_4^0 + B_4^2 \hat{O}_4^2 + B_4^4 \hat{O}_4^4 \qquad (1)$$

with the usual notation [10]. Here $S = 5/2$. The first term corresponds to the electronic Zeeman interaction, and the rest are the ZFS terms. The B_n^m-parameters are sometimes

expressed as $B_2^0 = \frac{1}{3}D = b_2^0$, $B_2^2 = E = \frac{1}{3}b_2^2$, $60B_4^0 = a/2 + F/3 = b_4^0$, and $B_4^4 = a/24 = \frac{1}{60}b_4^4$ [10]. The fine-structure splittings in the EPR spectra are mainly due to the second-order ZFS tensor, which can be expressed as

$$\mathbf{D} = \begin{pmatrix} -B_2^0 + B_2^2 & & \\ & B_2^0 - B_2^2 & \\ & & 2B_2^0 \end{pmatrix}. \tag{2}$$

The values of the ZFS parameters are given in table 1, together with those of the isoelectronic Mn^{2+} centres in NaCl and of the Fe^{3+}(IV) centre.

When the magnetic field is rotated in a (001) plane, the EPR lines can be divided into three groups: z-lines, resulting from Fe^{3+} centres oriented with the magnetic field parallel to the z-axis of the second-order ZFS tensor at 0° rotation angle ($\bar{H} \parallel \langle 100 \rangle$ direction), and x- and y-lines, for which the magnetic field is parallel to the x- and y-axes of the ZFS tensor at a rotation angle of 45° from the $\bar{H} \parallel \langle 100 \rangle$ direction (figure 1). The EPR transitions of the x- and y- lines are degenerate in a $\langle 100 \rangle$ direction.

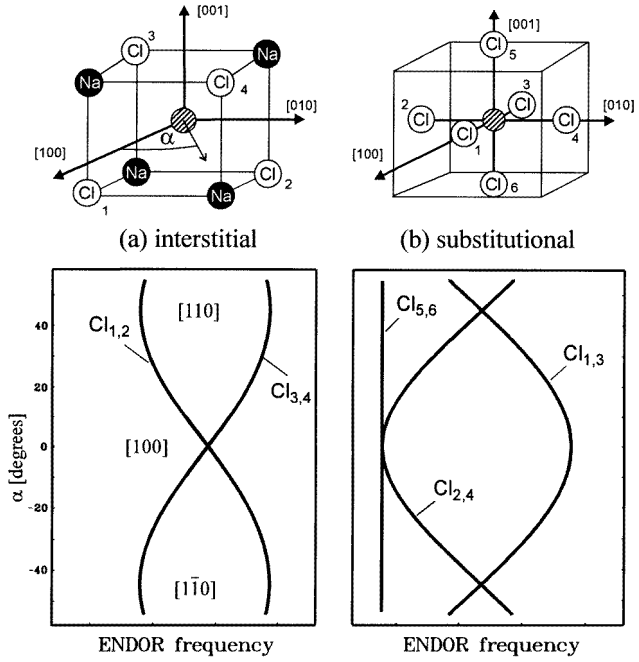

Figure 2. Calculated ENDOR angular variation of the first shell of ^{35}Cl, for two models of Fe^{3+} incorporation (interstitial and substitutional): only the lines of one m_S-manifold are shown, and the quadrupole and ZFS interactions are neglected.

3.2. ENDOR measurements

Compared to the case for the cubic Fe^{3+} centres studied previously [7], ENDOR measurements of the orthorhombic Fe^{3+}(I) centres are complicated by the fact that, due to the large ZFS parameters, the EPR transitions extend over a large magnetic field range and are highly anisotropic. The EPR lines labelled x, y, and z in figure 1 were chosen for the ENDOR measurements because in the X band they are well separated from the other

lines as well as from the EPR lines of the Fe^{+} centre. The x- and y-lines correspond to $m_S = 3/2 \leftrightarrow 5/2$ and the z-line to $m_S = -3/2 \leftrightarrow -5/2$ transitions if the sign of B_2^0 is assumed to be positive. The signal-to-noise ratio of the ENDOR spectra measured on the z-line decreased considerably when the magnetic field was rotated away from the ⟨100⟩ direction. Good ENDOR spectra could only be obtained for rotation angles up to about $\pm 3^\circ$. The whole ENDOR angular variation in the (001) plane could be obtained only for the x- and y-lines.

Table 2. Superhyperfine and quadrupole interaction parameters of the first- and second-shell neighbours of the Fe^{3+}(I) centre in NaCl (at $T = 15$ K). The values are given in MHz for the ^{35}Cl and ^{23}Na isotopes. The sign of the shf interaction is given relative to the sign of the axial ZFS parameter B_2^0. The relative signs of the quadrupole interaction and the shf interaction could only be determined for the Cl_5 shell. Θ is the angle between the z-axes of the shf and quadrupole interaction tensors of shells Cl_{1-4} and the cubic ⟨100⟩ and ⟨010⟩ axes. Positive values refer to a tilting towards the $\langle 1\bar{1}0\rangle$ axis. The estimated errors are: ± 0.02 MHz for the chlorine shells, ± 0.005 MHz for the sodium shells, and $\pm 1^\circ$ for the angles Θ_{SHF} and Θ_Q.

Shell	a/h	b/h	b'/h	q/h	q'/h	Θ_{SHF}	Θ_Q
$Cl_{1,2}$	−7.21	−2.32	−0.48	|1.50|	|0.10|	0.9	0.3
$Cl_{3,4}$	−9.00	−2.20	−0.68	|1.82|	|0.41|	0	0
Cl_5	−7.61	−2.59	−0.01	+1.60	+0.01	—	—
Na_I	−0.215	−0.145	0[a]	|0.133|	0[a]	—	—
Na_{II}	−0.106	−0.124	0	|0.104|	0	—	—
Na_{III}	−0.238	−0.524	0	|0.103|	0	—	—
Na_{IV}	−0.215	−0.451	0	|0.111|	0	—	—

[a] Note that for the Na_{I-IV} shells, the non-axial values of the shf and quadrupole interaction tensors were set to zero. The angular variation prevents us from determining all of the parameters of the shf and quadrupole interaction tensors.

3.2.1. First-shell ^{35}Cl. The analysis of the ENDOR angular variation measured on the x- or y-lines can answer the question of whether Fe^{3+} is incorporated substitutionally or interstitially. In the former case the plane of rotation contains the four nearest equatorial Cl^- neighbours (figure 2(b)). If we assume no lattice relaxation, the nn Cl^- ions should be equivalent at $\bar{\boldsymbol{H}} \parallel \langle 110\rangle$, and the shf and quadrupole interaction should have an extremum for one pair of neighbours in a ⟨100⟩ direction. In addition, there are axial nn Cl^- ions perpendicular to the plane of rotation. ENDOR lines corresponding to these nuclei should be almost independent of the rotation angle if the non-axial terms b' and q' of the shf and quadrupole interaction are small (see below).

In the interstitial case the Fe^{3+} should be surrounded tetrahedrally by the nn Cl^- ions (figure 2(a)), and therefore they should be equivalent for the magnetic field in a ⟨100⟩ direction with an extremum of the shf and quadrupole interaction at $\bar{\boldsymbol{H}} \parallel \langle 110\rangle$ in the (100) angular variation. The lower part of figure 2 shows simplified calculated ENDOR angular variations for the two cases: only the lines of one m_S-manifold are shown, and the quadrupole and fine-structure interaction as well as the angular dependence of the EPR spectrum (that would result in an angle-dependent Larmor frequency) are neglected.

Comparison with the experimental angular dependence in figure 3 shows that Fe^{3+} can only be at the substitutional site.

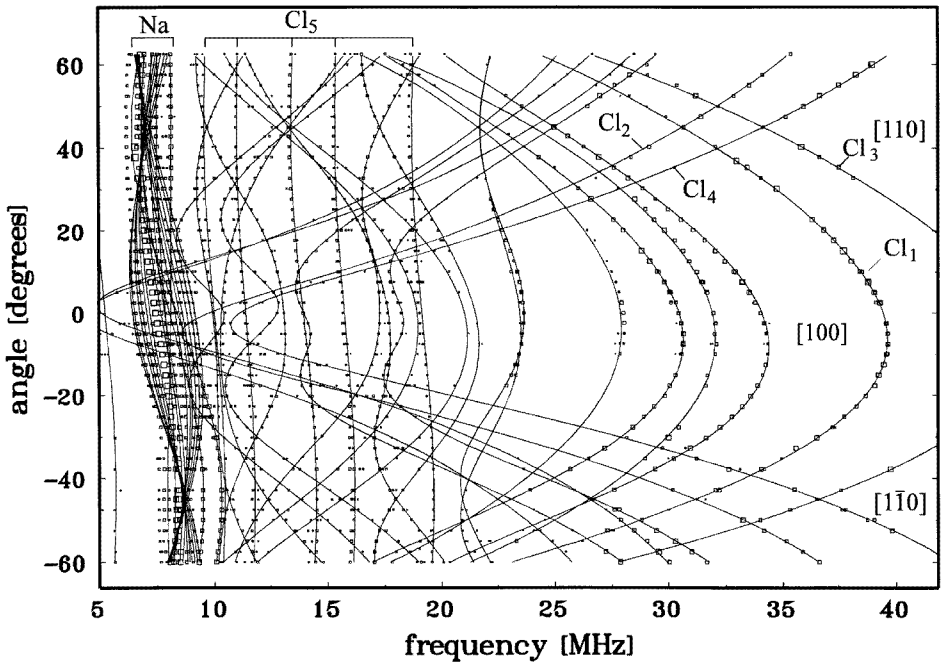

Figure 3. Angular variation of the ENDOR transitions due to shf interaction with the nn ^{35}Cl nuclei. The ENDOR spectra were measured on the x-EPR line (the $m_S = 5/2 \leftrightarrow 3/2$ EPR transition) of the Fe^{3+}(I) centre (see figure 1). The squares represent experimental line positions (the size indicates the line intensity), and the continuous lines represent the angular dependence calculated with the parameters of table 2.

The ENDOR spectra are quantitatively described by the following spin Hamiltonian:

$$\mathcal{H} = g\mu_B \boldsymbol{B}_0 \cdot \boldsymbol{S} + B_2^0 \hat{O}_2^0 + B_2^2 \hat{O}_2^2 + \sum_j (\boldsymbol{S}\hat{\mathbf{A}}_j \boldsymbol{I}_j + \boldsymbol{I}_j \hat{\mathbf{Q}}_j \boldsymbol{I}_j - g_{Ij}\mu_n \boldsymbol{B}_0 \cdot \boldsymbol{I}_j) \tag{3}$$

with the usual notation [10]. Here $S = 5/2$ and $I = 3/2$ for ^{23}Na, ^{35}Cl, and ^{37}Cl. The sum runs over the various Cl^- and Na^+ neighbours. The first term corresponds to the electronic Zeeman interaction, the second and third to the second-order ZFS terms, and the last three denote the shf, quadrupole, and nuclear Zeeman interactions, respectively. In order to obtain the shf and quadrupole interaction constants, the angular dependence calculated using the spin Hamiltonian (3) was compared with the experimental one of figure 3 and with one from the ENDOR spectrum measured on the z-line at $\tilde{\boldsymbol{H}} \parallel \langle 100 \rangle$. The solid lines in figure 3 are the ENDOR line positions calculated using the parameters from tables 1 and 2. The shf interaction constants are given in terms of the isotropic shf constant a and the anisotropic shf constants b and b', which are related to the principal values of the shf tensor by

$$A_{xx} = a - b + b' \qquad A_{yy} = a - b - b' \qquad A_{zz} = a + 2b. \tag{4}$$

In a similar way, the quadrupole interaction constants are related to the quadrupole tensor by

$$Q_{xx} = -q + q' \qquad Q_{yy} = -q - q' \qquad Q_{zz} = 2q. \tag{5}$$

The small difference, of the order of 40 kHz, between the calculated ENDOR frequencies and the measured line positions is probably due to the fact that the fourth- and sixth-order ZFS parameters were not included in the calculation.

We found that the four Cl^- nuclei in the plane of rotation (Cl_1 to Cl_4 in figure 2(b)) are split into two subshells with different shf and quadrupole interaction parameters (see table 2).

Some ENDOR lines in the frequency region between 10 and 20 MHz are almost isotropic when the ENDOR angular dependence is measured on the x- or y-line. Therefore these lines must be assigned to the axial Cl^- ions ($Cl_{5,6}$ in figure 2(b)) lying on an axis parallel to the z-axis of the ZFS tensor.

ENDOR lines due to interactions with the ^{37}Cl nuclei with lower abundance are seen as weak lines in the ENDOR spectra. The appearance of these lines at positions calculated using the ^{35}Cl data and the ratio of nuclear moments and nuclear quadrupole constants of ^{35}Cl and ^{37}Cl [10, 12] further supports the assignment of ENDOR transitions that we have chosen.

With the shf and quadrupole parameters of one axial chlorine subshell and two subshells of equatorial chlorines, all observed ENDOR lines in the region between 5 and 44 MHz due to ^{35}Cl and ^{37}Cl nuclei can be accounted for. However, from the analysis of the ENDOR spectra it is impossible to conclude whether the shell of axial chlorines consists of one nucleus or two nuclei on opposite sides of the substitutional Fe^{3+} ion. This information cannot be obtained either from a comparison of ENDOR line intensities of the different subshells, because of the large variation in transition probabilities.

3.2.2. Second-shell ^{23}Na. The ENDOR lines due to interactions with the sodium nuclei of the second shell appear in the frequency range from 5 to 12 MHz around the Larmor frequency of ^{23}Na (7.32 MHz at 650 mT). In figure 4 the angular dependence of these ENDOR ines is shown. Only the deviation from the Larmor frequency ν_K (set to 0 MHz) is shown.

As expected from symmetry considerations, the second shell of 12 Na^+ nuclei is split into several subshells. Four Na^+ ions are in the equatorial xy-plane, which is the plane of rotation.

We found that the shell of four equatorial Na^+ neighbours is split into two subshells (labelled I and II in figure 4) with different shf and quadrupole interaction parameters. In addition there are four sodium nuclei above and four below the xy-plane. The corresponding ENDOR lines are labelled as shells III and IV in figure 4. The values of the shf and quadrupole interaction parameters are given in table 2.

4. Discussion

On the basis of previous EPR results and the production and annealing properties of the Fe^{3+}(I) centres, two simple structural models of the precursor Fe^{2+}(I) centre seemed to be the most likely [4].

(a) An interstitial Fe^{2+} ion, with two nn charge-compensating cation vacancies in two corners of a tetrahedron.

(b) A substitutional Fe^{2+} ion with a neighbouring defect along a $\langle 001 \rangle$ direction, responsible for the strong axial crystal field experienced by Fe^{3+}.

The interstitial model in which the orthorhombic (local axes $\langle 110 \rangle$, $\langle 1\bar{1}0 \rangle$, $\langle 001 \rangle$) crystal field is generated by two nn cation vacancies, separated from the Fe^{2+} ion by a smaller

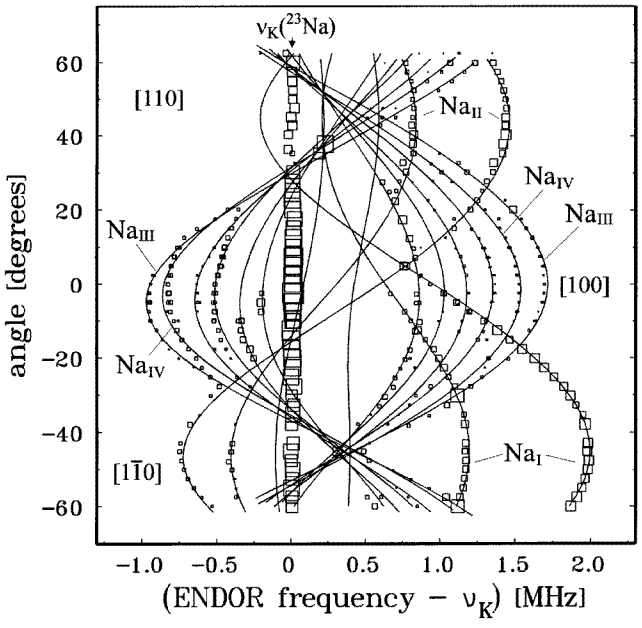

Figure 4. The angular variation of the ENDOR transitions due to shf interaction with the nn ^{23}Na nuclei. The ENDOR spectra were measured on the x-EPR line (the $m_S = 5/2 \leftrightarrow 3/2$ EPR transition) of the Fe^{3+}(I) centre (see figure 1). The frequency scale is shifted such that the ^{23}Na Larmor frequency corresponds to 0 MHz. The squares represent experimental line positions (the size indicates the line intensity), and the continuous lines represent the angular dependence calculated with the parameters of table 2.

distance than in the case of a substitutional Fe^{3+}, seemed very tempting. This model could explain in a straightforward manner both the formation of the interstitial Fe^{3+}_{cub} centre and the large ZFS of the low-temperature Fe^{3+} centres.

However, the analysis of the ENDOR spectra shows that the Fe^{3+} ion is incorporated on a substitutional site.

A simple model that provides both an axial crystal field and a local charge compensation for the substitutional Fe^{2+} would be a cation vacancy in a nnn position. Isoelectronic $Mn^{2+}v_c$(nnn) centres of such a configuration have been already observed [5] in NaCl:Mn crystals. The same structure has been attributed to the Fe^{3+}(IV) centres which are produced in small concentrations in chlorinated NaCl:Fe crystals after irradiation at LNT and subsequent annealing in the 153 K $< T <$ 185 K range [3, 4]. Indeed, the two centres exhibit the same ⟨001⟩ axial symmetry and similar values of the B_2^0-parameter, i.e. 0.004 52 cm^{-1} for $Mn^{2+}v_c$(nnn) and 0.004 83 cm^{-1} for Fe^{3+}(IV) [3–5].

The much larger value of $B_2^0 = 0.048\,91$ cm^{-1} for the Fe^{3+}(I) centre strongly suggests that the generating defect is much closer, probably at the site of one of the axial Cl^- in the first shell. This conclusion is further supported by an analysis of the parameter $B_2^0(b_2^0)$ with the superposition (SP) model [13]. According to the SP model, the ZFS parameters b_n^m are given by

$$b_n^m = \sum_i \bar{b}_n(R_i) K_n^m(\theta_i, \phi_i) \tag{6}$$

where the coordination factors $K_n^m(\theta_i, \phi_i)$ and the intrinsic parameters $\bar{b}_n(R_i)$ are functions

of the metal–ligand distance R_i for each impurity ion and the type and coordination of the ligands involved. It has been shown [14] that for Fe^{3+} ions with sixfold coordination by Cl^- ligands, one has

$$\bar{b}_2(R_i) = \bar{b}_2(R_0)\left(\frac{R_0}{R_i}\right)^7 \tag{7}$$

where $\bar{b}_2(R_0) = 0.61\ \text{cm}^{-1}$ for $R_0 = 0.219$ nm.

Considering the presence of a charge-compensating defect at one of the nn axial Cl^- sites, and neglecting in a first approximation the displacements induced in the first Cl^- shell by its presence, one finds $(B_2^0)_{calc} = \frac{1}{3}(b_2^0)_{calc} = 0.0370\ \text{cm}^{-1}$ for $R_i = 0.2798$ nm (the low-temperature lattice parameter of NaCl). The calculated value compares well with the experimental value of $(B_2^0)_{exp} = 0.0489\ \text{cm}^{-1}$. The difference can be easily accounted for by considering a decrease of only $\Delta R = 0.011$ nm in the Cl^-–Fe^{3+} distance. The decrease can be induced by the additional electrostatic interaction between the defect and the Fe^{3+} ion.

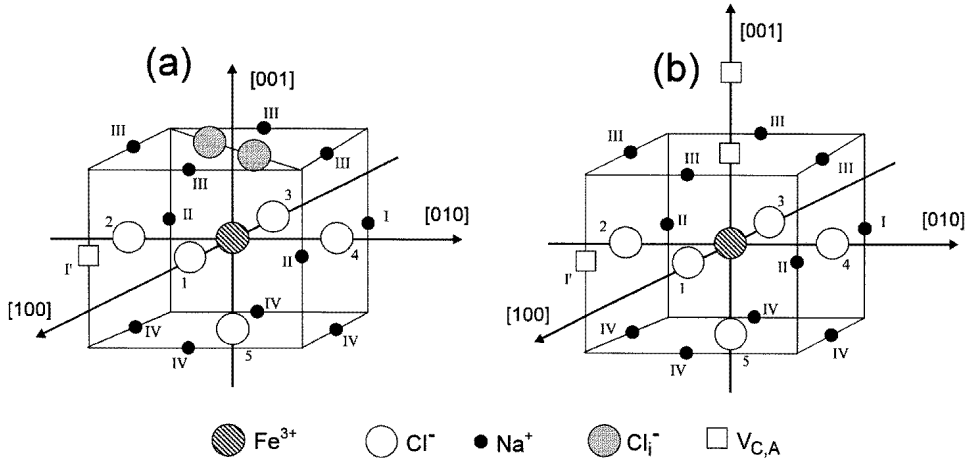

Figure 5. Two possible models for the Fe^{3+}(I) centre: (a) a split Cl_2^- interstitial is a nearest neighbour to Fe^{3+}_{subst}; (b) a divacancy is a nearest neighbour to Fe^{3+}_{subst}.

The defect at the nn axial Cl^- site may be an interstitial Cl_i^- ion which is pushing the adjoining substitutional Cl^- into a symmetrical position with respect to the ⟨001⟩ axis, along a ⟨110⟩ direction (figure 5(a)). A similar situation has been reported [15] earlier in the case of the $Pb^+(Cl_i^-)$ defect in KCl crystals. The resulting split interstitial also yields an orthorhombic crystal field with the required orientation of the local axes. However, in order to account for the different shf and quadrupole parameters of the two subshells of equatorial Cl^- ions (table 2), one has to consider in addition the presence of a sodium vacancy in the xy-plane. Its presence (site I′ in figure 5(a)) could also explain the observation that only two of the four equatorial Cl^- (Cl_1 and Cl_2) have a shf tensor axis tilted away from the ⟨100⟩ direction.

The charge-compensating split-interstitial defect requires the existence of another set of ENDOR lines from a second subshell of 'axial' Cl^-.

These ENDOR lines could have been identified by their angular variation. In contrast to the ENDOR lines of the Cl^- ions in the plane of rotation, the ENDOR lines due to

the Cl_i nuclei should have extrema when $\bar{\boldsymbol{H}} \parallel \langle 110 \rangle$. The anisotropy in the ENDOR angular variation would depend on the angle between the Fe^{3+}–Cl_i connection line and the z-direction ([001]) of the ZFS tensor. If the ionic radius of Cl^- is used to estimate the Cl–Cl separation, an angle of $\Theta_{shf} \approx 30^\circ$ would result. In spite of a careful search, no ENDOR lines with this angular behaviour were found.

Moreover, if we calculate the width of the EPR lines using the shf interaction parameters of the first chlorine shell, we find that 70% of the observed EPR linewidth can be accounted for. Therefore it is improbable that additional ENDOR lines due to an interstitial Cl^- ion occur at frequencies higher than 40 MHz, because this would broaden the EPR line too much.

Perhaps the absence of ENDOR lines from the split interstitial can be explained by a smaller shf interaction between the unpaired $3d^5$ electrons and the split-interstitial nuclei. This could result in ENDOR lines at lower frequencies that are obscured by lines due to the nn Na^+ and nnn Cl^- ions. A small shf interaction could be associated with a smaller overlap between the Fe^{3+} metal 3d orbitals (mainly $3d_{z^2}$) and the molecular $\sigma\pi$-orbitals of the split interstitial.

Another possible charge-compensating defect which, according to the SP model, may explain the EPR/ENDOR results, is a divacancy replacing one of the two axial chlorines from the first shell and the sodium ligand next to it along the same z-axis (figure 5(b)). In combination with a cation vacancy at site I′ in the second shell of equatorial sodium ligands, the orthorhombic symmetry of the Fe^{3+}(I) centre as well as the local charge compensation could be accounted for. The equatorial cation vacancy would also explain the presence of two distinct subshells of equatorial nn Cl^- ions, as well as the tilting of the shf tensor for the ligands Cl_1 and Cl_2 (table 2). Furthermore, this model only requires one shell of axial Cl^- ions.

The substitutional Fe^{3+} model with a split-interstitial Cl_i^- ion in the first shell is supported by the observation that the trapped-hole Fe^{3+}-type centres are produced only in NaCl:Fe crystals grown in a chlorine atmosphere, crystals which we know to contain an excess of chlorine, which is otherwise continuously released into the atmosphere, even at RT. The model is further supported by the identification [11] of a similar, so-called $Mn^{2+}I_z$ centre, with ZFS parameters comparable to those of the Fe^{3+}(I) centre (table 1). The $Mn^{2+}I_z$ centre has been considered to consist of a substitutional Mn^{2+} ion which has trapped an interstitial Cl_i^- ion produced by long-time radiolysis in its neighbourhood. This is not surprising, considering that in crystals grown conventionally a sizable increase in the concentration of interstitials can be obtained only by heavy irradiation with ionizing radiation [16].

The other model with a charge-compensating divacancy is also tempting, as it does not require any further ENDOR lines to be expected. However, in this case it is quite difficult to explain the role played by the chlorine atmosphere in the formation of the Fe^{2+}(I) centres.

The Fe^{3+}(I) centres are not directly converted into the cubic Fe^{3+} centres. Annealing above 245 K converts the Fe^{3+}(I) centres at first into the so-called Fe^{3+}(II) and Fe^{3+}(III) centres, before both centres decay above 280 K to form the Fe^{3+}_{cub} centres [4]. The Fe^{3+}(II) centres have an axial fine-structure component that is comparable in magnitude, but the orthorhombic perturbation of the ZFS tensor is smaller than for the Fe^{3+}(I) centres. The Fe^{3+}(III) centres are characterized by a considerably smaller axial ZFS component, but the orthorhombic component is of comparable size. In addition, the axis of the ZFS tensor is tilted out of the $\langle 100 \rangle$ direction by an angle of 3.7°.

Both substitutional models can explain the conversion of the Fe^{3+}(I) centres into cubic Fe^{3+}_{cub} centres in a straightforward manner. One can imagine the following steps. In the first

step the Fe^{3+} ion traps another cation vacancy in the second shell of sodium neighbours as soon as these become mobile. This will result in a smaller orthorhombic distortion and an almost equal axial field, as observed for the Fe^{3+}(II) centres. Subsequently the very small Fe^{3+} ion is attracted by the negatively charged cation vacancies, moving from the substitutional position into an interstitial position towards the sodium vacancies, leaving another sodium vacancy behind. The Fe^{3+} centre now consists of an interstitial Fe^{3+} ion with three sodium vacancies and either a Cl_2^- split interstitial or a divacancy. The resulting centre will still retain the same orthorhombic symmetry but a much smaller axial distortion, as observed for the Fe^{3+}(III) centres. This configuration of nearest neighbours is responsible for the orthorhombic fine-structure component as well as for the tilting of the fine-structure tensor axis. Further on, the interstitial iron repels the only remaining nearest-neighbour cation. For the full conversion into the cubic Fe^{3+} centre, the remaining interstitial chlorine moves away (interstitial charge compensation), or the chlorine vacancy is filled (the divacancy charge-compensating defect).

5. Conclusions

The ENDOR study of the Fe^{3+}(I) centres shows that during the growth of NaCl:Fe single crystals in a chlorine atmosphere a substantial fraction of the Fe^{2+} ions enter the NaCl lattice as Fe^{2+}(I) centres. Such centres consist of a substitutional Fe^{2+} ion with a charge-compensating defect at one of the nearest chlorine sites. The defect, which is responsible for the large axial second-order ZFS parameter B_0^2, may be either an interstitial Cl_i^- forming together with a nearest Cl^- neighbour a split interstitial, or a divacancy along the z-axis at adjacent nn Cl^- and nnn Na^- sites. At present, the available experimental data do not allow us to identify exactly the nature of the charge-compensating defect.

An additional cation vacancy in the equatorial plane is required to account in the case of a divacancy for the orthorhombic component of the ZFS, and in both cases for the different shf and quadrupole parameters of the two subshells of equatorial chlorines. The presence of a cation vacancy in the equatorial plane is expected to result in a small tilting of the local crystal-field axes of the Fe^{3+}(I) centre as well, which seems to be masked in the EPR spectra by the large axial distortion.

Acknowledgments

One of the authors (SVN) is indebted to the Deutscher Akademischer Austauschdienst (DAAD) for a three-month research scholarship to work at the University of Paderborn, Fachbereich 6—Physik, during the early stages of this study.

References

[1] Nistor S V, Velter-Stefanescu M and Mateescu D C 1985 *Solid State Commun.* **53** 989
[2] Yang B R, Bowen A and Schoemaker D 1985 *Phys. Status Solidi* b **127** 657
[3] Nistor S V, Ursu I and Velter-Stefanescu M 1986 *Phys. Status Solidi* b **135** K149
[4] Nistor S V, Ursu I and Velter-Stefanescu M 1987 *Cryst. Lattice Defects Amorph. Mater.* **17** 33
[5] Watkins G D 1959 *Phys. Rev.* **113** 79
[6] Nistor S V and Velter-Stefanescu M 1985 *J. Phys. C: Solid State Phys.* **18** 397
[7] Nistor S V, Pawlik T and Spaeth J-M 1995 *J. Phys.: Condens. Matter* **7** 2225
[8] Agullo-Lopez F, Catlow C R A and Townsend P D 1988 *Point Defects in Materials* (New York: Academic)
[9] Barb D, Constantinescu S, Nistor S V and Tarina D 1990 *Hyperfine Interact.* **53** 279
[10] Pilbrow J R 1990 *Transition Ion Electron Paramagnetic Resonance* (Oxford: Clarendon)

[11] Ikeya M, Itoh N and Suita M 1969 *J. Phys. Soc. Japan* **26** 291
[12] Spaeth J-M, Niklas J R and Bartram R H 1992 *Structural Analysis of Point Defects in Solids—An Introduction to Multiple Magnetic Resonance Spectroscopy (Springer Series in Solid State Sciences 43)* (Berlin: Springer)
[13] Newman D J and Ng B 1989 *Rep. Prog. Phys.* **132** 134
[14] Nistor S V, Goovaerts E and Schoemaker D 1994 *J. Phys.: Condens. Matter* **6** 2619
Nistor S V, Goovaerts E and Schoemaker D 1995 *Radiat. Eff. Defects Solids* **133** 191
[15] Goovaerts E, Nistor S V and Schoemaker D 1983 *Phys. Rev.* B **28** 3712
[16] Schoemaker D 1976 *Defects and their Structure in Nonmetallic Solids* ed B Henderson and A E Hughes (New York: Plenum) p 173